A study of the mechanical response of polycrystalline ice subjected to dynamic tension loading using the spalling test technique

Dominique Saletti, David Georges, Victor Gouy, Maurine Montagnat, Pascal Forquin

Highlights

- The spalling test technique is conducted to study the dynamic tensile strength of polycrystalline ice.
- The results show the sensitivity of the tensile strength to the applied strain rate (from 41 s^{-}1 to 271 s^{-}1).
- Three indicators are proposed to assess the results based on an optical analysis, a measurement of the wave speed and an analysis of the transmitted pulse.
- An increase of the cracking density with the strain rate is observed.

A study of the mechanical response of polycrystalline ice subjected to dynamic tension loading using the spalling test technique

Dominique Saletti[a], David Georges[a,b], Victor Gouy[b], Maurine Montagnat[b], Pascal Forquin[a]

[a] *Univ. Grenoble Alpes, CNRS, Grenoble INP[1], 3SR, F-38000 Grenoble, France*
[b] *Univ. Grenoble Alpes, CNRS, Grenoble INP[1], IGE, F-38000 Grenoble, France*

Abstract

Polycrystalline ice has been extensively investigated during the last decades regarding its mechanical behaviour for quasi-static loadings. Conversely, only few studies can be found on its dynamic behaviour and scientists suffer from a lack of experimental observation to develop relevant modelling at high strain-rate ranges. Dynamic experiments have already been conducted in compression mode using Hopkinson bar set-up. Regarding tension, experimental observations and measurements are scarce. The literature gives only approximated strength values. The knowledge of the latter is essential to design structures that may experience ice impact. The present study aims at providing the first reproducible experimental data of the tensile strength of polycrystalline ice subjected to dynamic tensile loading. To do so, a spalling test technique has been used for the first time on ice to apply tensile loading at strain-rates from 41 s^{-1} to 271 s^{-1}. The experimental results show that the tensile strength is sensitive to the applied strain-rate, evolving from

[1] Institute of Engineering Univ. Grenoble Alpes

1.9 MPa to 16.3 MPa for the highest applied loading rate.

Keywords: spalling test, ice, dynamic tensile strength, strain-rate sensitivity, fracture

1. Introduction

Ice found on Earth has a hexagonal crystallographic structure and is also known as ice Ih, the only stable phase at atmospheric pressure. The mechanical behaviour of its isotropic polycrystalline form (also called granular ice) has been widely investigated during the last decades but essentially regarding its mechanical response to static or quasi-static loading cases (Schulson and Duval [1]). In order to design structures that may experience ice impact, the knowledge of the mechanical response of ice experiencing dynamic loading is of main interest. To achieve this goal, some studies were conducted using different techniques. Two main characterisations can be found in the literature, one investigating the response of the material to dynamic compression loading and one looking at the response of a mechanical structure experiencing an ice ball impact. As far as the authors know, only one study, done by Lange and Ahrens [2], deals with the dynamic tensile behaviour of ice. In this work, ice specimens were tested in plate impact experiments and a tensile strength of about 17 MPa is measured at a strain-rate of $10^4 s^{-1}$. Regarding compression tests, a study was made by Combescure et al. [3] using a fast hydraulic jack allowing applied strain-rates from 10^{-2} s^{-1} to 50 s^{-1}. The ultimate compressive strength was identified to be 10 ± 1.5 MPa. Shazly et al. [4] investigated the compressive behaviour at a higher range of strain-rate (60 to 1400 s^{-1}) using a classical Hopkinson pressure bar with a short cylin-

drical specimen. The ultimate compressive strength was established to be around 15 MPa at the lowest strain-rates (60 s^{-1}) reaching about 58.4 MPa for the highest strain-rates(1400 s^{-1}). By changing the size of the specimen and the velocity of the striker, Kim and Keune [5] loaded the ice material at strain-rates from 400 s^{-1} to 2600 s^{-1}. Regarding the ultimate compressive strength, a mean value of 19.7 MPa was identified with values varying from 12 to 29 MPa. The authors stated a slight sensitivity to the strain-rate but the dispersion of the results cannot allow assessing this fact firmly.

Some clues on the dynamic behaviour of ice can also be found from the studies that used ice impact on mechanical structures (Combescure et al. [3], Pernas-Sánchez et al. [6]). The results obtained from these tests are mostly used to validate numerical modelling of ice ball impact on different types of structures and, then, do not propose a direct identification of tensile strength values for ice itself.

Except the work of Lange and Ahrens [2], all the studies investigating the tensile strength of ice propose values at strain-rate ranges that do not exceed 10^{-3} s^{-1}. Both Schulson [7] and Petrovic [8] proposed a general review of the mechanical properties of ice in which tension is described. According to Schulson [7], the fracture in tension is due to a transgranular cleavage with a maximal applied strength around 1 MPa. The same value is given by Petrovic [8] and does not seem to be influenced by the applied strain-rate, at least up to 10^{-3} s^{-1}. In fact, the main parameter influencing the tensile behaviour of ice appears to be the grain size of the material and the temperature. The tensile strength decreases when grain diameter increases, with the existence of a critical grain diameter for which a brittle-to-ductile fracture transition

occurs. This critical grain diameter appears to decrease with the increase of the applied strain-rate. Despite all these pieces of information about the mechanical response of polycrystalline ice to tensile loadings, the strain-rate sensitivity can only be presumed: no data are available for strain-rate above 1 s^{-1}.

Understanding the dynamic tensile behaviour of the polycrystalline ice is of main interest since tension plays an important role in the damage process of a material subjected to impact and having a quasi-brittle behaviour (Forquin and Hild [9]) such as ice. Among all the mechanical parameters that should be investigated and identified in order to get satisfying modelling, the tensile strength is at the forefront. But experimentally speaking, applying a tensile loading can be very difficult, especially with materials as polycrystalline ice for which the attachment to the possible grips is tricky. Specimens cannot be threaded or glued, except with water, but in that case, the test has to be carefully designed in order for the failure to remain in the center part of the specimen and not at the boundaries. In addition, the experimental set-ups that can be found in the literature to apply dynamic tensile loading to quasi-brittle materials are limited to a range of 1 s^{-1} to 1000 s^{-1}. Universal testing machines equipped with fast hydraulic jack can reach strain-rate up to 1 $s^{-1}$and the Split Hopkinson Tensile Bars technique can lead to loading rates up to 200 s^{-1}(Cadoni et al. [10], Saletti et al. [11]) but for both cases, the specimen attachment is problematic due to likely melting of ice at contact surfaces. Indeed, a stress should be applied on the specimen surface transmitting the tensile forces during the test. This stress could lead to a temperature variation of the specimen and melt locally the

material, preventing the forces to be transmitted. Xia and Yao [12] made a complete review of the different techniques to apply a tensile loading to brittle materials such as rocks which have, as well as polycrystalline ice, a higher strength in compression than in tension. The Brazilian test technique could be employed but the authors propose here what seems to be a good candidate to tackle the issue of applying a dynamic tensile loading: the spalling testing technique. This technique needs a specimen with a simple cylindrical shape and only a simple unilateral contact with the measurement bar (Klepaczko and Brara [13], Erzar and Forquin [14]). Furthermore, it applies an homogeneous stress state in the section of the specimen.

This paper aims at understanding the behaviour of polycrystalline ice submitted to tension by measuring at the tensile strength of the material and its sensitivity to the strain-rate. In a first part, the investigated material and the experimental setup along with its processing are presented in details. Then the results are analysed and discussed before concluding on a strain-rate sensitivity of the tensile strength of polycrystalline ice submitted to high strain rates..

2. Material and method

2.1. Specimen preparation

21 polycrystalline ice specimens were prepared in order to obtain isotropic granular ice, characterized by nearly equiaxed grains and an isotropic crystallographic texture. To do so, the well-known technique described in Barnes et al. [15] was applied. Seeds obtained from crushed dionised clean water ice are put into a mould within which vacuum is performed. Dionised and

degassed water at 0 $°C$ is gently poured into the mold, and freezing is performed from bottom to top. Vacuum is released at the end of the freezing stage. Specimens are maintained at -5 $°C$ for more than 24h for relaxation. This method provides granular ice specimens of density between 900 and 917,7 $kg.m^{-3}$ (at -5 $°C$), with no visible bubble, and an average mean grain diameter of 1 to 2 mm (this diameter depends on the size of the initial seeds).

After lathing and milling, 120 mm-long cylindrical specimens have been obtained with a diameter of $45^{+0.3}_{-1.4}$ mm and two campaigns have been carried out. The first one includes specimens #LP01 to #LP13 and the second one, specimens #LP14 to #LP21. The mean grain size of the specimens is 1.52 ± 0.44 mm and the densities are given at a temperature of -15 $°C$. According the expression for the temperature dependence of the density of ice (Gammon et al. [16]), the reference value is 919,3 $kg.m^{-3}$ at -15 $°C$. Here, the calculation of the density using the mass and volume of the specimen delivers a typical uncertainty of individual values about $\Delta\rho = \pm 5$ $kg.m^{-3}$. The 21 samples used in the frame of the spalling test campaigns are listed in Table 1 with their specific dimensions and characteristics.

Crystallographic isotropy of the different specimens has been checked by the analyses of thin sections performed on ice pieces extracted at one side of the specimens, before lathing. Ice is a birefringent material, and this property enables to extract the optical axis (which corresponds to the long axis of the hexagonal crystallographic structure, also called c-axis) by observing transparent thin section of ice between cross polarisers. The crystallographic c-axis orientation distribution is obtained by making use of an Automatic

Table 1: Dimensions and densities of the specimens used in this study. The uncertainty for the measurements of the densities is estimated at about $\pm 5\ kg.m^{-3}$.

Spec Id	LP01	LP02	LP03	LP04	LP05	LP06	LP07	LP08	LP09	LP10	LP11
Length (mm)	119.4	120.3	119.8	120	119.9	117.9	120.2	120	119.6	119.2	120
Diameter (mm)	44.9	45	45	44.7	45	45	43.6	45	45.2	45	45
Density ($kg.m^{-3}$)	917	920	916	913	905	908	920	921	926	915	916

Spec Id	LP12	LP13	LP14	LP15	LP16	LP17	LP18	LP19	LP20	LP21
Length (mm)	118.6	120	119.7	119.9	120.1	119.9	119.6	119.2	120	120.6
Diameter (mm)	45	44.9	45.1	45.1	45.1	45	45.1	45	45.3	45.2
Density ($kg.m^{-3}$)	915	917	906	917	922	908	912	906	910	918

Ice Texture Analyzer described by Wilson et al. [17]. Typical thin section dimensions are about $4 \times 8\ cm^2$ size, and 0.3 μm thickness obtained in several cross-section of the analysed specimen. The distribution of the c-axis orientations and the microstructure obtained for one representative specimen is represented on Figure 1a. One can observe that there is no preferred c-axis orientation in the specimen and grains are equiaxed.

In addition, micro-computed tomography has been conducted on one specimen (voxel size of 14 μm in this case) to evaluate the manufacture of the specimen regarding the presence of pores. The result is presented on Figure 1b in which it can be observed that the porosity of the specimen is very low. Quantitative analyses of scans from various regions of the specimen led to a density for pores exceeding 1mm in diameter of about $10^{-3}\ mm^{-3}$.

2.2. Spalling test technique

The Hopkinson-bar-based spalling test technique is generally used to investigate the dynamic tensile strength of quasi-brittle materials from a few tens of s^{-1} to about 200 s^{-1}. This experimental set-up is made of a short projectile and a slender Hopkinson bar at the end of which the contact with the specimen is made. All the parts are cylindrical with approximately the same diameter. The test creates a short compressive pulse with the projectile propagating in the slender bar and into the specimen. This pulse is reflected into a tensile pulse at the free-end of the specimen, propagating in the opposite direction and applying tension (Erzar and Forquin [14, 18, 19], Klepaczko and Brara [13], Schuler et al. [20]). This test is well suited for materials that have a higher compressive strength than tensile strength which is the case for polycrystalline ice, according to the literature, at least for quasi-static load-

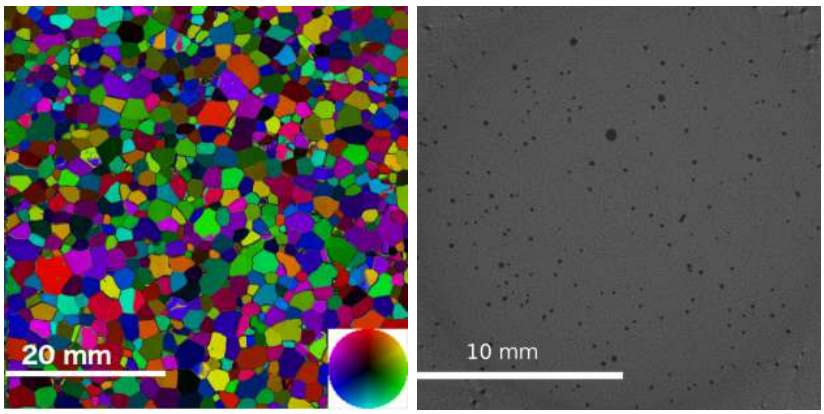

(a) (b)

Figure 1: (a) C-axis orientation colour-coded microstructure (see colour-wheel on the bottom right) of specimen #LP06. (b) Slice view of an X-ray micro-tomography of a specimen obtained with the protocol defined in section 2.1. The darkest grey level refers to voids. The scanned area corresponds to the centre of a cross-section of the specimen located at its mid-height. The voxel size is 14 μm^3.

ing rates. The set-up used for these experiments is described in Figure 2. The projectile and the Hopkinson bar are made of high-strength aluminum (7xxx series, yield strength $> 450\ MPa$), which has a 1D wave speed C of 5078 $m.s^{-1}$, a density of 2800 $kg.m^{-3}$ and a Youngs modulus equal to 72.2 GPa. The diameter of the two components is 45 mm and the bar is 1200 mm long. The projectile is 50 mm long and has a spherical-cap-ended nose (radius of 1.69 m) to act as a pulse shaper in order to smooth the loading pulse Readers are invited to consult (Erzar and Forquin [14]) in which this technique is fully investigated. The Hopkinson bar is instrumented with a strain gauge to measure the compressive pulse applied to the specimen. A reflective paper is fixed (thanks to frozen water) at the free-end of the speci-

men allowing the measurement of the particle velocity of this rear face thanks to a laser interferometer from Polytec company, enabling velocity measurements up to 20 $m.s{-}1$ with a minimum bandwidth of 1.5 MHz (Erzar and Forquin [14]). This bandwidth is necessary due to the fact that a spalling test experiment lasts for a hundred of microseconds.

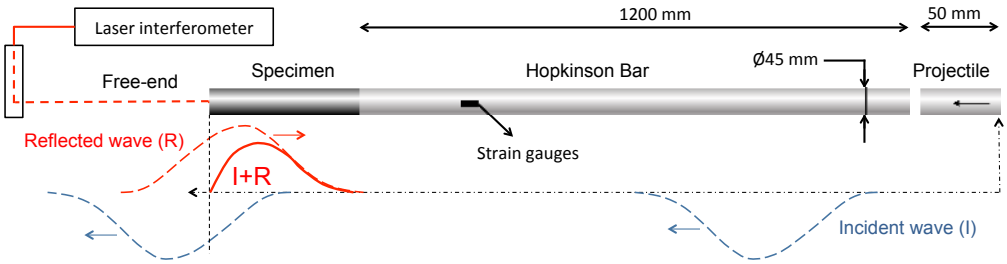

Figure 2: Scheme of the spalling test set-up used in the experiments.

The temperature of the test is an important point. The first idea would be to use a cooled box to assess an accurate temperature around the specimen just before the test. This solution is not suitable here: the only measurement instrumentation on the specimen being the reflective paper at its free-end, the used of an ultra-high-speed (UHS) camera is essential. Then, using a cooling box would prevent capturing good quality images during the test and measuring the particle velocity of the rear face of the specimen with the laser interferometer. A compromise has been made. The specimens are stored in a deep-freezer near their final position in the experimental set-up. A protocol has been established in order to ensure that less than 30 seconds elapse between the time when the specimen is taken out from the deep-freezer and the time when it is loaded by the spalling test apparatus. This duration has been determined experimentally by doing some trials. A

numerical simulation (using a finite-element software) confirmed that no noticeable warming occurs inside the specimen during 30 s. In particular, the simulated temperature remains constant in the spalled region. A thin frost layer can be observed at the surface of the specimen when taking it out from the freezer but it does not seem to have an influence on the test.

During the specimen preparation in the cold room, a cylinder made of the same aluminium alloy as the input bar is glued by mean of frozen water on the specimen. Then, the assembly is put into a deep-freezer set to $-30\ ^{\circ}C$ at least the night before the tests. This cylinder is 45 mm in diameter and three lengths were used, 10 mm, 30 mm and 40 mm. Its main roles are (i) to avoid a thermal shock between the ice specimen and the Hopkinson bar which is at room temperature; (ii) to delay the melting of the specimen on its bar side face, which would lead to an impedance discontinuity between the bar and the specimen by the creation of a thin film of water, preventing the load from being correctly transmitted ; (iii) and finally, the position set-up of the specimen, in contact with the input bar, is facilitated. First because an aluminium/aluminium contact has to be set instead of a ice/aluminium one. Second because we designed, on this aluminum cylinder, a holding system made of three pins equally spaced that are connected to pins on the bar by means of springs. This method ensures the best contact between the aluminium cylinder fixed on the specimen, and the bar. The forces applied by the springs are very low and the stress wave propagation is only influenced on its way back, in tension. At this time, the specimen is already broken.

3. Test processing

3.1. Measurement of the tensile strength

Classically, the spalling test technique allows identifying the tensile strength of a material if the assumption of an elastic macroscopic behaviour with no damage of the material before the stress peak is valid (Erzar and Forquin [14], Schuler et al. [20]). In that case, the tensile strength corresponds to the spalling stress leading to the first crack in the specimen and is identified by using the Novikov's formula as expressed in equation 1 (Novikov et al. [21]).

$$\sigma_{spall} = \frac{1}{2}\rho_{specimen} C_{specimen} \Delta V_{pb} \tag{1}$$

where ΔV_{pb} is the pullback velocity corresponding to the difference between the maximum velocity and the velocity at rebound that are measured on the rear face of the specimen, σ_{spall} is the spalling stress leading to fracture (MPa), $\rho_{specimen}$ is the specimen density ($kg.m^{-3}$) and $C_{specimen}$ is the elastic wave speed in uniaxial stress state given by $C_{specimen} = \sqrt{E_{specimen}/\rho_{specimen}}$ where $E_{specimen}$ refers to the elastic modulus of the material specimen. By using this formula, an implicit assumption is made: the celerity of waves in the polycrystalline ice is the same for compressive and tensile waves. The velocity rebound indicates a tensile damage occurring in the specimen during the test. A schematic way to measure it is described in Figure 3. The descending part of the velocity profile corresponds to the tensile phase of the test.

Due to the assumptions made in order to establish equation 1 and due to experimental difficulties, several indicators were defined and measured for each test in order to declare it valid or not. These indicators are the wave

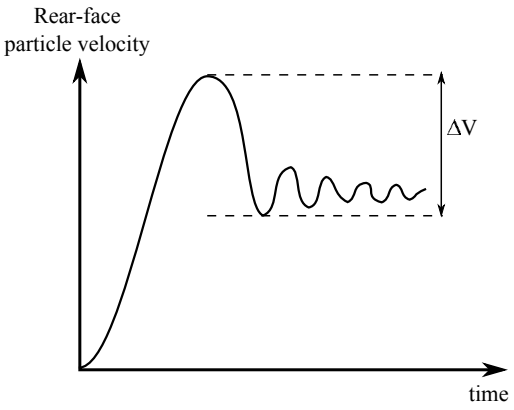

Figure 3: Velocity rebound measurement.

speed in the specimen, the transmitted stress ratio σ_T/σ_I in the specimen, σ_T and σ_I respectively standing for the transmitted and the incident stresses and the qualitative observation of the crack pattern in the specimen during the test based on high speed photography. Each point is described in the following sections.

3.2. Measurement of the wave speed in the specimen

Equation 1 allows obtaining the tensile strength of the specimen. Two features of this equation are linked to material properties of the specimen. In the present case, the density of the specimen is quite well known and measured during the specimen preparation. Regarding the wave speed C, one can consider it as constant. As explained in equation 1, it depends on the density as well as E which refers to the elastic modulus in one-dimensional uniaxial stress-state. In the present case, the specimen is made of homogeneous ice aggregates which are composed of randomly oriented grains, resulting in an elastic isotropic behaviour (Schulson and Duval [1]). For this case, at $-16\ ^{\circ}C$, according to Gammon et al. [16], $E_{ice} = 9.33\ GPa$. This value was

obtained by exploiting the propagation of sound waves in ice, allowing obtaining a so-called dynamic elastic modulus. In the current study, this result is considered as a reference and, due to this assumption, here, no influence of strain-rate was studied for this parameter.

But it is also possible to determine the wave speed from the experiments by using the strain gauge and the interferometer signal. Both are an image of the applied loading, respectively in the bar and in the specimen (one can refer to equations 5 and 6). The idea is to determine the travel time between the strain gauge and the free end of the specimen in order to determine the wave speed. To do so, it is necessary to render the two signals dimensionless and both positive. Then, a cross-correlation analysis is made on the rising stage of the signal. From this analysis, one can obtain Δt which represents the time delay between the two signals. Then the wave speed in the specimen, $C_{specimen}$, is obtained by equation 2:

$$C_{specimen} = \frac{l_{specimen}}{\Delta t - \frac{l_{gauge\_to\_bar\_end}}{C_{bar}}} \tag{2}$$

where $l_{specimen}$ is the specimen length, $l_{gauge\_to\_bar\_end}$ is the length from the gauge to bar-specimen interface, including the intermediate aluminium alloy and C_{bar} is the wave speed in the bar.

Besides the fact that $C_{specimen}$ is used to compute the spalling stress (equation 1), this measurement can also be a good indicator of the quality of the contact between the specimen and the bar during the test by checking if its value is reasonable in comparison with an *a priori* standard value of ice of :

$$C_{ice} = \sqrt{\frac{E_{ice}}{\rho_{ice,(T=-30\ ^\circ C)}}} = \sqrt{\frac{9.33\ GPa}{921.6\ kg.m^{-3}}} = 3182\ m/s \tag{3}$$

where $\rho_{ice,(T=-30\ ^\circ C)}$ is the corrected density of ice according the expression for the temperature dependence of the density of ice (Gammon et al. [16]).

3.3. Bar to specimen transmitted stress ratio

The impedance of the bar section and of the specimen section can be expressed as $Z = S\rho C$ with S the cross-section, ρ the density of the material, C its one-dimensional wave speed. Improving the impedance match between the bar and the specimen allows obtaining stress levels high enough in the specimen to damage it during a test, while maintaining the Hopkinson bar and the projectile in their elastic domain. According to the elastic wave propagation theory in the case of a change of impedance section and assuming that the contact is perfect between the bar and the specimen, the ratio α between the incident stress σ_I coming from the bar and the transmitted stress σ_T created in the specimen can be expressed as in equation 4:

$$\alpha = \frac{\sigma_T}{\sigma_I} = \frac{2}{\frac{Z_{bar}}{Z_{specimen}} + 1} \tag{4}$$

where $Z_{bar} = S_{bar}\rho_{bar}C_{bar}$ and $Z_{specimen} = S_{specimen}\rho_{specimen}C_{specimen}$.

Then α can be used as a quality indicator for the spalling tests performed in this study. The impedance $Z_{specimen}$ can be computed for each test leading to a theoretical value α_0 which can be compared to α_{exp}, the ratio value obtained by measuring σ_I and σ_T in a time interval containing the stress peak in compression.

The bar remaining in the elastic domain, the measurement of the strain ϵ_{gauge} at the gauge location in the bar and the knowledge of the bar's Young modulus allow measuring σ_I. σ_T is obtained by the particle velocity measurement $V(t)$ prior to the velocity rebound. Equations 5 and 6 are used:

$$\sigma_I(t) = E_{bar}\epsilon_{gauge}(t) \tag{5}$$

$$\sigma_T(t) = \frac{1}{2}\rho_{specimen}C_{specimen}V(t) \tag{6}$$

α_{exp} is determined in the compression phase. The evaluation of the test is done by calculating the ratio α_{exp}/α_0 . A value around 1 means that the contact between the bar and the specimen is close to being perfect and the closer to 0 the ratio, the lower the quality of contact. If the contact is not good, it does not necessarily mean that the test should not be considered. The input stress is not completely transmitted but the specimen is still undergoing compression and tension. Often, in this case, the particle velocity from the rear face of the specimen is too far from the expected shape idealised in Figure 3, making impossible to use equation 1, and so the tensile strength cannot be deduced.

3.4. Qualitative test checking with an Ultra High Speed camera

An important point of the spalling test experiment is that the specimen has to remain undamaged during the compressive loading phase. This is usually reachable due to the strong compressive strength compared to the dynamic tensile strength of quasi-brittle materials tested with this apparatus. In the present case, the projectile impact velocity needs to be carefully

estimated, in order to get strain-rate in the expected range and to ensure that the compressive stress applied to the specimen does not exceed the compressive strength value given by the literature, otherwise the assumption made to use the particle velocity is not valid, making the measurement of the tensile strength impossible. The review done by Schulson and Duval [1] reported a compressive strength around 10 MPa at 10 s^{-1} for specimens made of fresh-water granular ice in unconfined configuration. Simple elastic numerical simulations of the test were conducted. The aim was to determine the initial projectile velocity to be considered in order to prevent failure due to a compression loading during the test. Then, during the experimental campaigns, the experiments are conducted at different impact velocities to apply different strain-rates.

To check if no damage or failure occured during the compression stage, we used an UHS camera (Kirana model from Specialised Imaging). For each test, 180 images with an inter-frame time of $1\mu s$ are obtained to visualise the compressive and tensile stages. Due to the transparent properties of ice, one can observe qualitatively the cracks appearing and propagating in the specimen. A test was considered successful if no compression fracture was visible near the contact after analysis of the sequence of images captured with the UHS camera. This point can be very challenging due to the fact that UHS cameras offer a very limited number of pixels in comparison with low speed and reflex cameras. Here, the Kirana model is equipped with one of the biggest sensor regarding the number of pixels (at the time of the study) with 924-by-768 pixels.

Figure 4 presents two different cases. On Figure 4a, no crack is visible in

the first compressive stage of the test. T_0 stands for the first picture captured by the UHS camera, a few μs before the compressive pulse reaches the specimen. Time $T_0 + 40\mu s$ corresponds approximately to the time at which the maximum compressive stress spreads the specimen in the contact zone. At time of $T_0 + 80\mu s$, which is fully within the tension stage, fractures are visible and can be linked to the applied tensile loading to the specimen. Conversely, on Figure 4b,a fracture prematurely occurs during the compression at a time of $T_0 + 40\mu s$. Then, at a time of $T_0 + 80\mu s$, fractures due to tension are visible.

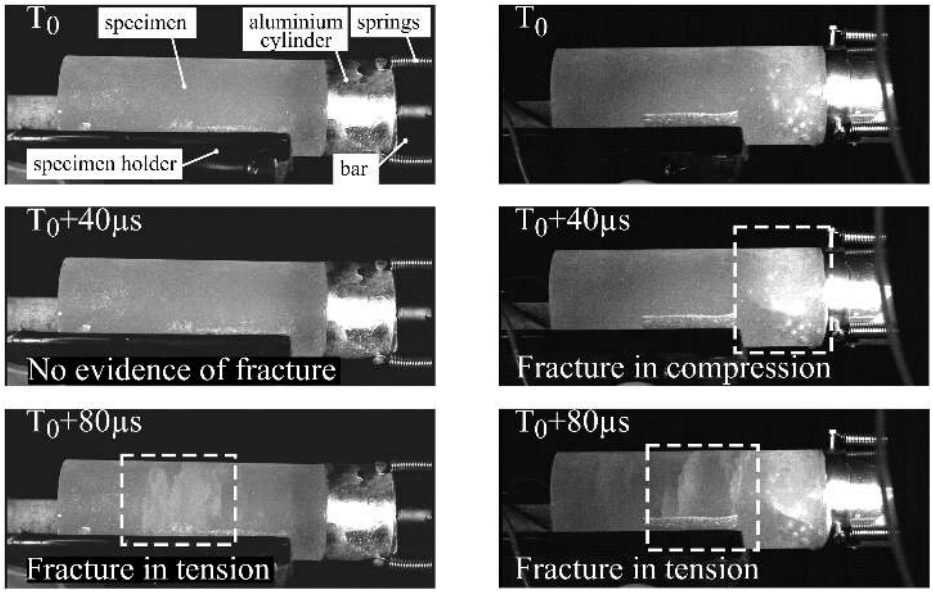

(a) Test visually sucessful. (b) Failed test.

Figure 4: Examples of two series of images obtained from two spalled specimens. (a) No crack in compression is visible, the fracture occurs in tension (test on specimen $\#LP20$. (b) A premature fracture in compression appears ($T_0 + 40\ \mu s$) then fracture in tension ($T_0 + 80\ \mu s$).

3.5. Determining the applied strain-rate during tensile stage

The last measure to be extracted from the spalling test is the applied strain-rate during the tension stage prior to the tensile damage. The identification method used to measure it is based on elastic numerical simulations. For each test, the velocity profile is artificially converted into an elastic profile. This is achieved by using the rear-face velocity measurement up to the rebound due to spalling. After this point, this curve is virtually prolongated keeping the slope of the tensile phase before spalling fracture. An example is given in Figure 5a. This velocity is converted into a stress using equation 7 :

$$\sigma_T(t - \Delta t) = \frac{1}{2}\rho_{specimen} C_{specimen} V(t) \tag{7}$$

In this formula $V(t)$ is the velocity history measured by the laser interferometer, ΔT the traveling time of the wave through the specimen and $\sigma_T(t - \Delta t)$ the stress which is supposed to be applied at the bar side of the specimen. This stress is used as a loading pulse in the numerical simulation. The exact density and dimensions of each specimen was used for each computation. Figure 5b shows the type of curve obtained from the simulation to evaluate the strain-rate. For each test, the values are extracted from the results of the numerical simulation at the approximate location of the first appearance of cracks, thanks to the image sequence filmed during the test. The curve is valid up to the spall strength identified with equation 1. To get the minimum, maximum and mean value of the strain-rate, we considered the stress interval beginning with the tensile phase ($\sigma > 0$) and ending with σ_{spall}. This interval is highlighted in grey in Figure 5b.

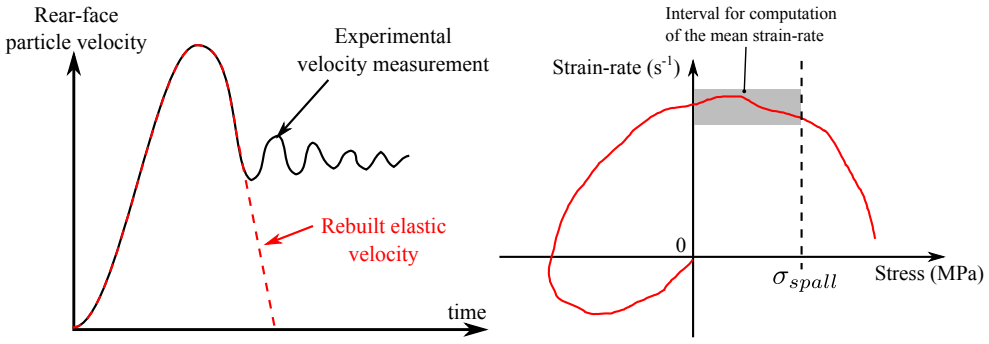

Figure 5: (a) Rebuilt of the rear-face velocity to reproduce an virtual elastic loading in numerical simulations. (b) Interval of data taken into account to compute the mean strain-rate of a test.

4. Results and discussion

4.1. Validity of the results

The main results are presented in Table 2.

Tests #LP03, #LP07 and #LP09 were eliminated from this table due to the fact that premature fractures in the compression stage occurred. By looking at the wave speed values, it can be noticed that tests #LP12, #LP13 have very low values of one-dimensional wave speed in comparison with the reference value of $C_{ice} = 3182m/s$ and should not be considered. For this reason, the corresponding data are highlighted in dark grey in the table. Regarding α_{exp} values, 7 tests have values quite low in comparison with the theoretical one α_0 (#LP01, #LP02, #LP04, #LP05, #LP06, #LP10 and #LP11), which means that the quality of the contact during these tests is really poor. Those results are highlighted in light grey in Table 2. Conversely, for the other tests, the α_{exp}/α_0 ratio is around 1, representing a good contact.

Table 2: Summary of the obtained results (dark grey: very low values of one-dimensional wave speed, light grey: low values of alpha, italic: result to be confirmed by further investigations.)

Spec Id #	C_{spec} (m/s)	α_{exp} (%)	α_{exp}/α_0 (%/%)	σ_{spall} (MPa)	$\dot{\epsilon}_{mean}$ (s^{-1})	$\dot{\epsilon}_{min} - \dot{\epsilon}_{max}$ (s^{-1})
LP01	3236	22,9	0,67	4,9	71	59-75
LP02	3389	16,7	0,47	3,1	34	24-37
LP04	2830	24,5	0,8	3,8	109	102-113
LP05	3189	19,6	0,58	3,4	49	36-53
LP06	2970	25,5	0,8	4,7	103	96-108
LP08	*3499*	*42,7*	*1,16*	*16,3*	*271*	*255-283*
LP10	3121	16,2	0,49	2,1	38	33-40
LP11	2978	21,3	0,67	3,3	89	81-93
LP12	2382	14,4	0,54	2,5	81	71-88
LP13	2235	6,3	0,25	1,4	51	47-54
LP14	3040	33,5	1,03	4,3	107	91-116
LP15	2654	27,3	0,93	1,9	41	37-44
LP16	2917	33,2	1,05	4,0	121	107-131
LP17	2992	33,1	1,04	4,4	110	99-117
LP18	2962	34,0	1,07	4,1	108	95-115
LP19	2881	33,0	1,07	4,3	120	111-126
LP20	3009	34,5	1,08	3,8	83	74-88
LP21	2793	32,5	1,07	3,2	69	58-76

This fact can be explained by the experimental technique that has been used. Indeed, it was mentioned that two campaigns were conducted for this study. In the first campaign, we set up the specimen on the bar by a simple unilateral contact with no force maintaining this contact. Great care was taken about the position of the specimen and the way to hold it before and during the test and rubber was applied around the intermediate aluminium alloy part and the bar end to prevent some movement. Unfortunately, this way of doing produces very random results on the quality of the contact as it is shown here. Nevertheless, some tests ran well but the setting-up position technique was changed between the two campaigns. In the second one, three springs equally distributed around the bar perimeter applying low-level forces were used to maintain the contact. The quality of the contact, as it can be seen in Table 2 is far more repeatable. Finally, for all the reasons mentioned above, it has been decided to only take into account the results that are not shadowed in Table 2 : only about 50% of the tests were considered as successful. The result obtained with #LP08 has to be confirmed by further investigations.

4.2. Tensile strength results

On the 9 tests considered here, the strain-rate applied is ranged between 41 and 271 s^{-1}. The variation of strain-rate was obtained by having different levels of projectile velocity impact. It can be noticed than the highest value of strain-rate is quite far from the rest of the measured strain-rates. This is due to the fact that only few tests with a high impact velocity of projectile were tried and only one worked out. In the other cases, contact issues or prematurely compressive failure occurred. Finally, the measured spalling stresses, i.e. tensile strengths, range from 1.9 to 16.3 MPa.

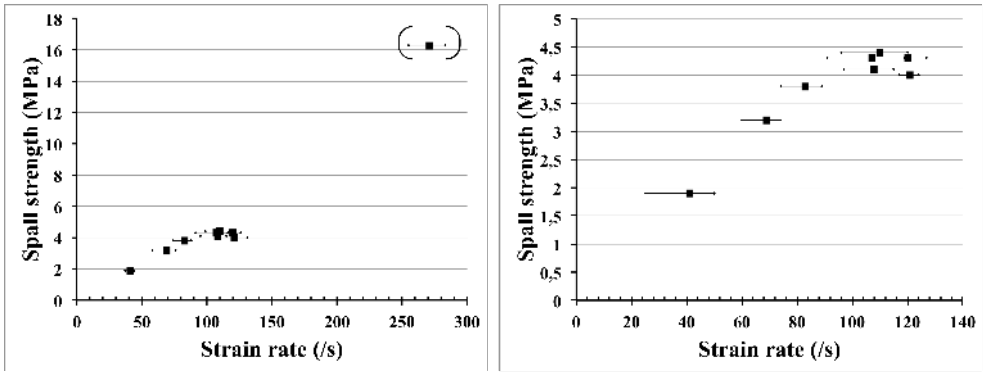

(a) (b)

Figure 6: Tensile strength measurements as a function of strain rate. The shown points indicate the mean values of determined strain-rates. The displayed intervals do not correspond to error bars. They correspond to the minimum and maximum values of strain-rate estimated during the tensile phase.(a) Taking into account #LP08 specimen. (b) Without #LP08 specimen.

Figure 6a summarises these results in one single graph. As it can be seen in this graph, the influence of the strain-rate on the tensile strength is clearly established. In addition, the obtained values are quite consistent with the reference value of 1 MPa in the quasi-static regime. As the highest point should be confirmed in further investigations, a focus on strain-rates up to 120 $s^{-1}$is presented in Figure 6b. The next logical step of this study would be to spread the test configuration over the full range of strain-rates to better establish the dynamic increase of the tensile strength of polycrystalline ice between the quasi-static and the dynamic regime.

403 *4.3. Qualitative analysis of the fracture*

404 The use of the UHS camera allowed us detecting premature fracture in
405 compression as well as observing the crack propagation in the volume of
406 the specimen during each test. Even if the latter is a qualitative piece of
407 information, it enables to distinguish three main scenarios as a function of
strain-rate, depicted in Figure 7.

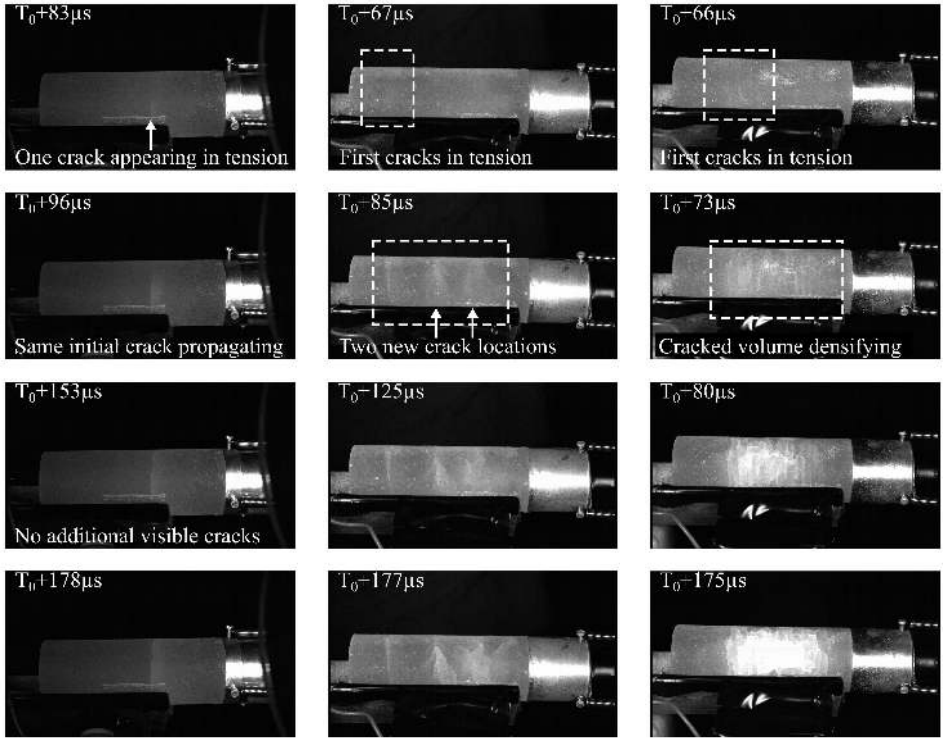

(a) #LP15 (41 s^{-1}) (b) #LP21 (69 s^{-1}) (c) #LP17 (110 s^{-1})

Figure 7: Fracture in the specimen for three different strain-rates. The evolution of the number of cracks clearly visible with the UHS camera increases with the strain-rate.

408

409 Test #LP15 was one of the tests conducted with the lowest value of mean
410 strain-rate. In the four pictures presented in Figure 7a, only one macro crack

can be observed. By contrast, at higher strain-rates such as in Figure 7c (test #LP17), several cracks oriented perpendicularly to the specimen axis develop in a small volume delimited by the white dashed-line rectangle at $T_0 + 66\mu s$. In the next steps of the test, this zone of damage spreads out towards the bar side of the specimen as observed on the last image where the light saturates. The cracks can be attributed to tensile loading. Finally, the higher the loading rate, the higher the number of cracks activated, which is consistent with the behaviour expected for brittle materials (Forquin and Hild [9]).

The result obtained on #LP21 is also interesting. Four images of this test are given in Figure 7b. The mean strain-rate is about 69 s^{-1}. In that case, three distinct cracked zones appear successively during the tensile phase following the propagation of the reflected tensile wave. The rate of the applied strain-rate being lower than in test #LP17, less cracks have been triggered.

5. Conclusions

This paper presents a first study to evaluate the tensile strength of polycrystalline ice subjected to strain-rates ranging from 41 to 271 s^{-1}. This was achieved by adapting the spalling test technique to polycrystalline ice. The experimental procedure is carefully presented and three indicators are proposed to validate each test: a qualitative optical analysis with an ultra-high-speed camera, a quantitative measurement of the wave speed in the material and a quantitative analysis of the quality of the contact with the α ratio (transmitted stress over incident stress). 21 specimens were prepared and 9 tests were considered to present the final results based on the Novikov

approximation. The results show that tensile strength is clearly influenced by the strain-rate: at strain-rates around 30 s^{-1} the tensile strength is found to be about 2 MPa, which is twice the quasi-static value reported in the literature (Schulson [7], Petrovic [8]). For strain-rates around 100 s^{-1}, the tensile strength is found to be around 4 MPa. The analysis of the fracture patterns occurring in the specimen during the test confirms also the elastic brittle behaviour of polycrystalline ice in tension of ice in this range of strain-rates.

Acknowledgements

The present work was developed in the framework of the Brittle's Codex chair (Fondation UGA) and thanks to the support from the CEA-CESTA (France) and from the Labex OSUG@2020 (ANR 10 LABEX 56). The provided support and fundings are gratefully acknowledged by the authors.

References

[1] E. Schulson, P. Duval, Creep and fracture of ice, Cambridge University Press, doi:https://doi.org/10.1017/CBO9780511581397, 2009.

[2] M. Lange, T. Ahrens, The dynamic tensile strength of ice and ice-silicate mixtures, Journal of Geophysical Research 88 (B2) (1983) 1197–1208, doi:https://doi.org/10.1029/JB088iB02p01197.

[3] A. Combescure, Y. Chuze-Marmot, J. Fabis, Experimental study of high-velocity impact and fracture of ice, International Journal of Solid and Structures 48 (2011) 2779–2790, doi: https://doi.org/10.1016/j.ijsolstr.2011.05.028.

[4] M. Shazly, V. Prakash, B. Lerch, High strain-rate behavior of ice under uniaxial compression, International Journal of Solid and Structures 46 (2009) 1499–1515, doi:https://doi.org/10.1016/j.ijsolstr.2008.11.020.

[5] H. Kim, J. Keune, Compressive strength of ice at imact strain rates, Journal of Materials Science 42 (2007) 2802–2806, doi: https://doi.org/10.1007/s10853-006-1376-x.

[6] J. Pernas-Sánchez, J. Artero-Guerrero, D. Varas, J. López-Puente, Analysis of ice impact process at high velocity, Experimental Mechanics 55 (2015) 1669–1679, doi:https://doi.org/10.1007/s11340-015-0067-4.

[7] E. Schulson, Brittle failure of ice, Engineering Fracture Mechanics 68 (2001) 1839–1887, doi:https://doi.org/10.1016/S0013-7944(01)00037-6.

[8] J. Petrovic, Review of mechanical properties of ice and snow, Journal of Materials Science 38 (2003) 1–6, doi: https://doi.org/10.1023/A:1021134128038.

[9] P. Forquin, F. Hild, A Probabilistic Damage Model of the Dynamic Fragmentation Process in Brittle Materials, Advances in Aplied Mechanics 44 (2010) 1–6, doi:https://doi.org/10.1016/S0065-2156(10)44001-6.

[10] E. Cadoni, D. Forni, R. Gieleta, L. Kruszka, Tensile and compressive behaviour of S355 mild steel in a wide range of strain rates, The European Physical Journal Special Topics 227 (2018) 29–43, doi: https://doi.org/10.1140/epjst/e2018-00113-4.

[11] D. Saletti, S. Pattofatto, H. Zhao, Measurement of phase transformation properties under moderate impact tensile loading in

a NiTi alloy, Mechanics of Materials 65, ISSN 01676636, doi: https://doi.org/10.1016/j.mechmat.2013.05.017.

[12] K. Xia, W. Yao, Dynamic rock tests using split Hopkinson (Kolsky) bar system – A review, Journal of Rock Mechanics and Geotechnical Engineering 7 (1) (2015) 27 – 59, ISSN 1674-7755, doi: https://doi.org/10.1016/j.jrmge.2014.07.008.

[13] J. R. Klepaczko, A. Brara, Experimental method for dynamic tensile testing of concrete by spalling, International Journal of Impact Engineering ISSN 0734743X, doi:https://doi.org/10.1016/S0734-743X(00)00050-6.

[14] B. Erzar, P. Forquin, An Experimental Method to Determine the Tensile Strength of Concrete at High Rates of Strain, Experimental Mechanics ISSN 00144851, doi:https://doi.org/10.1007/s11340-009-9284-z.

[15] P. Barnes, D. Tabor, J. C. F. Walker, The Friction and Creep of Polycrystalline Ice, Proceedings of the Royal Society A: Mathematical, Physical and Engineering Sciences ISSN 1364-5021, doi: https://doi.org/10.1098/rspa.1971.0132.

[16] P. H. Gammon, H. Kiefte, M. J. Clouter, W. W. Denner, Elastic constants of artificial and natural ice samples by Brillouin spectroscopy., Journal of Glaciology ISSN 00221430, doi: https://doi.org/10.1017/S0022143000030355.

[17] C. J. Wilson, D. S. Russell-Head, H. M. Sim, The application of an automated fabric analyzer system to the textural evolu-

503 tion of folded ice layers in shear zones, Annals of Glaciology doi:
504 https://doi.org/10.3189/172756403781815401.

505 [18] B. Erzar, P. Forquin, Experiments and mesoscopic modelling of dy-
506 namic testing of concrete, Mechanics of Materials ISSN 01676636, doi:
507 https://doi.org/10.1016/j.mechmat.2011.05.002.

508 [19] B. Erzar, P. Forquin, Analysis and modelling of the cohesion strength of
509 concrete at high strain-rates, International Journal of Solids and Struc-
510 tures ISSN 00207683, doi:https://doi.org/10.1016/j.ijsolstr.2014.01.023.

511 [20] H. Schuler, C. Mayrhofer, K. Thoma, Spall experiments for the measure-
512 ment of the tensile strength and fracture energy of concrete at high strain
513 rates, International Journal of Impact Engineering ISSN 0734743X, doi:
514 https://doi.org/10.1016/j.ijimpeng.2005.01.010.

515 [21] S. Novikov, D. I.I., I. A.G., The study of fracture of steel, aluminium
516 and copper under explosive loading, Fizika Metallov i Metallovedenie 21
517 (1966) 608.